# Prediction of the Structure of Fuel Sprays in Cylindrical Combustion Chambers

Jian-Shun Shuen*
*Sverdrup Technology Inc./NASA Lewis Research Center, Cleveland, Ohio*

**The structure of fuel sprays in cylindrical combustion chambers is theoretically investigated using computer models of current interest. Three representative spray models are considered: 1) a locally homogeneous flow (LHF) model, which assumes infinitely fast interphase transport rates; 2) a deterministic separated flow (DSF) model, which considers finite rates of interphase transport but ignores effects of droplet/turbulence interactions; and 3) a stochastic separated flow (SSF) model, which considers droplet/turbulence interactions using stochastic methods. Various flow conditions are considered to examine the influence of droplet size and swirl strength on the spray flame structure. Comparison of calculated results with the experimental data shows that general features of the flow structure can be predicted with reasonable accuracy using the two separated flow models. In contrast, the LHF model overpredicts the rate of development of the flow. It is found that large swirl is associated with a high rate of evaporation and intensive turbulent mixing and combustion. Increased droplet diameter produces a longer flame length and reduces combustion intensity when compared to smaller initial droplet diameters.**

## Nomenclature

$C_D$ = drag coefficient
$d_p$ = droplet diameter
$f$ = mixture fraction
$g$ = mean square of mixture fraction fluctuations
$k$ = turbulence kinetic energy
$m_p$ = droplet mass
$\dot{n}_i$ = number flow rate of droplets in group $i$
$P(f)$ = probability density function (PDF) of $f$
$r$ = radial distance
$r_0$ = combustion chamber radius
$S$ = swirl number
$S_\phi$ = source term
$S_{p\phi}$ = droplet source term
$T$ = temperature
$u$ = axial velocity
$V_j$ = volume of computational cell $j$
$v$ = radial velocity
$w$ = tangential velocity
$x$ = axial distance
$\Gamma$ = exchange coefficient
$\epsilon$ = rate of dissipation of turbulence kinetic energy
$\rho$ = density
$\phi$ = generic property
$\Psi$ = scalar property

*Subscripts*

$p$ = droplet property
0 = initial condition
$\infty$ = ambient property

*Superscripts*

$(\bar{\ })$ = time-averaged quantity
$(\tilde{\ })$ = Favre-averaged quantity
$(\vec{\ })$ = vector quantity

Received April 1, 1986; revision submitted June 30, 1986.

*Senior Research Engineer.

## Introduction

THE objective of this investigation is to evaluate liquid fuel spray combustion models for gas turbine combustors and furnaces. Reviews by Crowe,[1] Law,[2] Faeth,[3] and Sirignano[4] discuss important aspects of spray modeling that are currently being addressed. Recent spray models differ in specific details, but generally may be divided into two categories: locally homogeneous flow (LHF) models and separated flow (SF) models.

LHF models represent the simplest treatment of a multiphase flow and have been widely used to analyze sprays.[5,6] The key assumption of the LHF model is that interphase transport rates are fast in comparison to the rate of development of the flow. This implies that all phases have identical properties at each point in the flow. Clearly, LHF models are only formally correct for flows containing infinitely small droplets. It was found[3,5,6] that, while LHF models provide a reasonable qualitative description of the flow structure, they generally overestimate the rate of development of the flow.

Numerous SF models have been proposed to consider interphase transport phenomena. Gosman and Johns[7] have divided them into three groups: discrete droplet models, continuous droplet models, and continuum formulation models. In the discrete droplet models,[1,3,8,9] droplets are divided into representative groups whose trajectories are tracked by solving the Lagrangian equations that govern droplet transport. In the continuous droplet models,[10] the droplets are represented by a statistical distribution function in a multidimensional space of droplet size, velocity, location, and time. The properties of droplets are determined by solving the conservation equation of the distribution function. In the continuum formulation models,[11] droplets are treated as a continuous fluid, so that the gas and droplets are represented as interpenetrating continua. This formulation requires one droplet fluid phase for each droplet size. In most recent spray models, the discrete droplet approach has been adopted, since it reduces numerical diffusion while providing a convenient framework for dealing with multiple droplet size and complex interphase transport phenomena.

Many discrete droplet models neglect the effects of turbulence on interphase transport.[1,3,9] This implies that droplets follow deterministic trajectories, yielding the deter-

ministic separated flow (DSF) model. Neglecting the effects of turbulence on droplet transport is appropriate when characteristic droplet relaxation times are large in comparison to characteristic times of turbulent fluctuations. Few practical sprays, however, satisfy this condition. Dukowicz[12] and Gosman and Ioannides[8] have adopted stochastic methods to study droplet dispersion by turbulence. Faeth and co-workers[13-17] extended the analysis of Gosman et al. to include the effects of turbulence on interphase heat and mass transport. Their stochastic separated flow (SSF) model[13-17] has been evaluated in a wide variety of parabolic flows with very encouraging results.

The present investigation extends the analyses of Refs. 13-17 to consider swirling and recirculating flows. Special emphasis is given to the influence of the initial droplet size distribution and inlet swirl strength on the spray flame structure. The effects of the finite interphase transport rates and droplet/turbulence interactions on flame properties are studied by comparing the results of the LHF, DSF, and SSF models with experimental data. Due to the complex nature of the flows considered and the uncertainties in both the predictions and the measurements, the study focuses on the qualitative features of the spray flames (rather than quantitative comparisons).

## Theoretical Methods

The LHF model is equivalent to the analysis of a variable density single-phase flow. The effects of the dispersed phase appear in the upstream boundary conditions and the representation of state relationships. The present LHF model is very similar to that reported in earlier work on evaporating and combusting sprays.[16,17]

### Gas Phase

The major assumptions of the gas-phase formulation are as follows: 1) the flow is steady, axisymmetric, and swirling; 2) exchange coefficients of all species and thermal energy are the same; 3) kinetic energy of the mean flow is negligible; 4) combustion is diffusion controlled; 5) radiative heat transfer is neglected; and 6) the sprays are dilute so that the influence of droplets on turbulence properties and the displacement of the gas by the droplets can be neglected. Favre-averaged governing equations are solved. The conserved-scalar formalism is used to obtain scalar properties. Turbulence closure is achieved by employing a $k$-$\epsilon$-$g$ turbulence model.[16,17]

The governing equations of the gas phase can be written in the general form,[9]

$$\frac{\partial}{\partial X}(\bar{\rho}\tilde{u}\tilde{\phi}) + \frac{1}{r}\frac{\partial}{\partial r}(r\bar{\rho}\tilde{v}\tilde{\phi}) = \frac{\partial}{\partial X}\left[\Gamma\frac{\partial\tilde{\phi}}{\partial X}\right] + \frac{1}{r}\frac{\partial}{\partial r}\left[r\Gamma\frac{\partial\tilde{\phi}}{\partial r}\right] + S + S_{p\phi} \tag{1}$$

where $\tilde{\phi} = \bar{\rho}\bar{\phi}/\bar{\rho}$ is the Favre-averaged dependent variable. The expressions for the exchange coefficient $\Gamma$ and the source term $S$ are widely available in the literature, e.g., Refs. 9 and 11. The term $S_{p\phi}$ is used for the SF model and represents the interaction between the droplets and the gas phase and is obtained from the droplet trajectory calculations.

A gaseous diffusion flame structure is assumed for the combustion analysis and the droplets are treated as distributed sources of fuel vapor. The presence of envelope flames around or wake flames behind individual droplets is neglected, since the majority of droplets spend most of their lifetimes in fuel-rich regions. Experimental confirmation of this assumption can be found in Refs. 3, 17, 18, and the references cited therein.

The Favre-averaged scalar properties are calculated from the probability density function (PDF) of mixture fraction $P(f)$ and state relationships of scalar properties as a function of mixture fraction $\psi(f)$,

$$\tilde{\psi} = \int_0^1 \psi(f)\tilde{P}(f)\mathrm{d}f \tag{2}$$

and $\bar{\rho}$ is found from

$$\bar{\rho} = \left(\int_0^1 \frac{1}{\rho(f)}\tilde{P}(f)\mathrm{d}f\right)^{-1} \tag{3}$$

A clipped Gaussian function is assumed for $\tilde{P}(f)$ and the most probable value and variance are determined by $\tilde{f}$ and $g$. The SSF model requires the time-averaged PDF, $P(f)$, which can be found as

$$\bar{P}(f) = \bar{\rho}/\rho(f)\tilde{P}(f) \tag{4}$$

State relationships are obtained by thermodynamic equilibrium calculations using the CEC-76 computer program developed by Gordon and McBride.[19] The partial equilibrium method is used for high mixture fraction conditions, following Ref. 20. For the LHF model in the region where liquid is present, phase equilibrium is considered in the construction of the state relationships. Details of this calculation can be found in Ref. 21.

### Droplet Phase

The liquid phase is treated by solving Lagrangian equations of motion and transport for the life histories of a statistically significant sample of individual droplets. This involves dividing the droplets into $n$ groups (defined by position, velocity, and diameter) at the fuel nozzle exit and then computing their subsequent trajectories in the flow. The major assumptions and the governing equations involved in the droplet transport calculations have been discussed in detail by Law,[2] Faeth,[3] and Shuen et al.[13-17] and will not be repeated here.

Time-averaged gas properties and instantaneous eddy properties should be used for droplet trajectory calculations in the DSF and SSF models, respectively. Time-averaged scalar properties can be found directly from the conserved-scalar formulation.[22] However, to convert Favre-averaged velocities to time-averaged velocities requires correlations of velocity-density fluctuations. To avoid undue complications in the analysis, the Favre-averaged gas velocities are used in the calculations. Jeng and Faeth[20] estimated the difference between the two averaged velocities in their diffusion flame to be less than 5%.

### Droplet/Turbulence Interaction

In the SSF model, the effects of turbulence on droplet transport are treated by a stochastic approach. The droplets are assumed to interact with a random distribution of eddies along their trajectories. The eddy properties are obtained by random sampling of the PDFs of velocity and mixture fraction. To simplify the analysis, velocity and mixture fraction are assumed to be statistically independent. The turbulence is assumed to be isotropic and to have a Gaussian PDF in the velocity fluctuations. Although the time-averaged PDF should strictly be used, the Favre-averaged PDF of velocity is used here for the same reason as in the DSF analysis.

The scalar eddy properties are obtained by sampling the time-averaged PDF, $P(f)$, for an instantaneous value of $f$ and then obtaining the corresponding scalar properties from the state relationships. The droplet/eddy interaction time is assumed to be the minimum of either the eddy lifetime or the transit time for the droplet to cross the eddy. Details of the specifications of these times and their calibration can be found in Refs. 13-17.

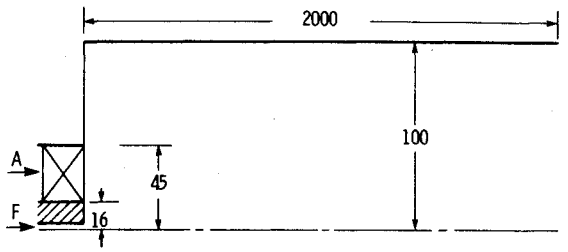


**Fig. 1 Geometry of the combustion chamber, Khalil et al.[25] (all dimensions in mm).**

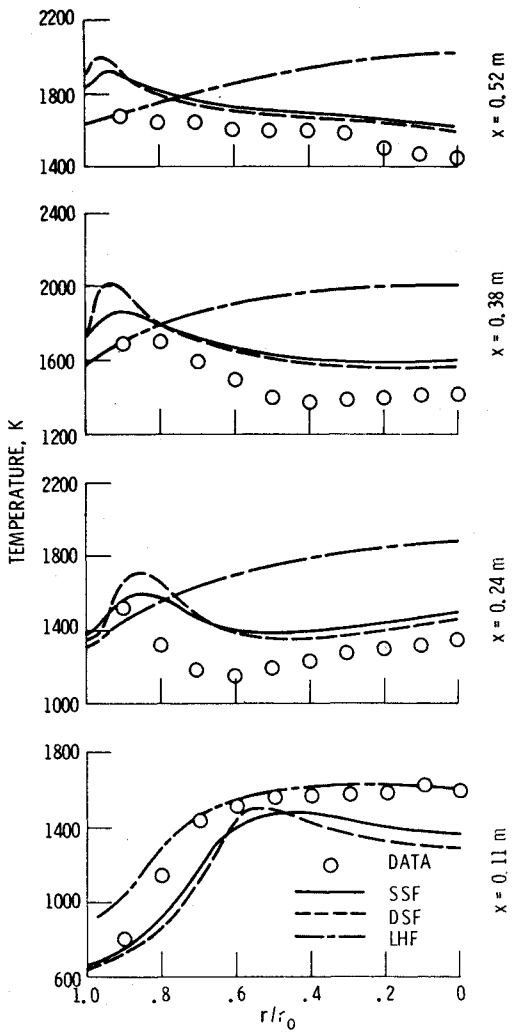


**Fig. 2 Radial profiles of temperature, $S=0.72$.**

### Droplet Source Terms

The mass and axial momentum source terms for each computational cell $j$ are calculated from the net change of droplet mass and axial momentum for each droplet group traversing this cell, as follows:

$$S_{pmj} = V_j^{-1}\left[\sum_{i=1}^{n} \dot{n}_i \left(m_{pi_{\text{in}}} - m_{pi_{\text{out}}}\right)\right]_j \tag{5}$$

$$S_{puj} = V_j^{-1}\left[\sum_{i=1}^{n} \dot{n}_i \left((m_{pi}u_{pi})_{\text{in}} - (m_{pi}u_{pi})_{\text{out}}\right)\right]_j \tag{6}$$

The droplet radial and tangential momentum source terms, however, cannot be calculated in this manner because of the additional force terms in the respective droplet equations of motion in the cylindrical coordinates. These source terms are obtained by directly computing the change of radial and tangential momentum due to drag, as follows:

$$S_{pvj} = V_j^{-1}\int_{t_{\text{in}}}^{t_{\text{out}}} \left(\sum_{i=1}^{n} \frac{3}{4}\dot{n}_i m_{pi}\frac{\rho}{\rho_p d_p}C_D \times (v_{pi}-v)\left|u_{pi}-u\right|\right)dt \tag{7}$$

$$S_{pwj} = V_j^{-1}\int_{t_{\text{in}}}^{t_{\text{out}}} \left(\sum_{i=1}^{n} \frac{3}{4}\dot{n}_i m_{pi}\frac{\rho}{\rho_p d_p}C_D \times (w_{pi}-w)\left|u_{pi}-u\right|\right)dt \tag{8}$$

### Boundary and Initial Conditions

Uniform profiles of mean gas-phase axial velocity and temperature are prescribed at the inlet. Inlet radial velocity is taken as zero and the tangential velocity is specified to have a solid-body rotation profile. Second derivatives of all dependent variables are assumed to be zero at the exit. Axisymmetry is assumed and nonslip conditions are specified along all solid surfaces. Wall cooling was applied to the combustion chambers in the experiments considered in the following sections. The amount of cooling applied or the wall heat flux, however, was not available and, therefore, the adiabatic wall condition was used in the calculations. This would cause overprediction of the near-wall temperatures.

Spray calculations are very sensitive to the droplet initial condition specifications.[9,13-17] The initial spray conditions required in the present analysis include droplet velocities, location, and size distribution. This information however, is rarely available in practical flows. As a result, approximations of initial conditions are used in the predictions. Initial droplet locations and velocities are estimated from the limited available experimental information. The droplet size is assumed to have either a Rosin-Rammler or a uniform size distribution. Upon impingement on a wall, the droplets are assumed to bounce back elastically and specularly. More specific droplet initial conditions pertinent to the individual experiments are given in the Results and Discussion section.

### Numerical Solution Procedure

A modified version of the TEACH computer program is used to solve the gas-phase governing equations. It includes an improved finite-difference procedure, the bounded skew-upwind differencing scheme (BSUDS) developed by Syed et al.[23] The pressure field is estimated using the pressure implicit operator (PISO) predictor-corrector technique developed by Issa.[24] The numerical error analysis of these schemes can be found in Ref. 24. The axisymmetric flow domain is divided into a relatively fine mesh, i.e., $60\times60$. For the separated flow analysis, the ordinary differential equations governing the droplet motion and transport are integrated using a fourth-order Runge-Kutta method. In all cases, 450 and 4500 trajectories are computed for the DSF and SSF models, respectively. The solution procedure follows the particle-source in cell (psi-cell) iterative method of Crowe.[1] The CPU time requirements are approximately 400, 800, and 2900 s, respectively, for the LHF, DSF, and SSF models on a Cray X-MP computer. In order to assess the grid dependence of the numerical solution, a coarser ($40\times40$) and a finer ($80\times80$) mesh are also used in some of the calculations. The maximum discrepancies in local flow properties are within 4% between the coarser and the base ($60\times60$) meshes and 2% between the base and the finer meshes. Therefore, we may conclude that the results of the $60\times60$ mesh are sufficiently close to a mesh-independent solution.

## Results and Discussion

### Measurements of Khalil et al.[25]

The theoretical models described in the previous sections were applied to the liquid-fueled furnace experiments reported by Khalil et al.[25] The same experimental data have been used by El-Banhawy and Whitelaw[9] to evaluate a deterministic separated flow spray model. Only one swirl number ($S=0.72$) was considered and a relatively coarse grid, i.e., $20\times 20$, was used in Ref. 9. An extensive sensitivity study was conducted, however, by these authors[9] to examine the effects of droplet size distribution and droplet initial velocity on the flow structure. In the present study, two swirl numbers ($S=0.72$ and 1.98) were considered. A Rosin-Rammler droplet size distribution, having an initial Sauter mean diameter (SMD) of 127 $\mu$m and 15 size groups with sizes of 10–290 $\mu$m, was assumed. The initial mass fraction of each size range is calculated using the expression

$$\Delta m=\frac{\delta d_p^{\delta-1}}{\bar{d}_p}\exp\left[-\left(\frac{d_p}{\bar{d}_p}\right)^{\delta}\right]\Delta d_p$$

where $\delta=2$, $\Delta d_p=20$ $\mu$m, and $\bar{d}_p=225$ $\mu$m. The droplet injection velocities were taken from Ref. 9, i.e., $u_p=11.0$ m/s, $w_p=6.1$ m/s, and $v_p=0.5$–$2.5$ m/s, the smallest value corresponding to the smallest droplet diameter. The geometry of the combustion chamber is shown in Fig. 1. Liquid kerosene was used as fuel and the fuel/air mass ratio was fixed at 0.0496.

The predicted and measured temperature profiles at different axial locations are given in Fig. 2 for $S=0.72$. The results show that both the DSF and SSF models underpredict the temperature in the near-inlet region, while the LHF model overpredicts the temperature, especially at large radii ($r/r_0>0.8$). The discrepancies between the predictions of the two separated flow models and the measurements are due to the underestimation of droplet spreading and evaporation. Results from a sensitivity study indicate that this underestimation is caused by uncertainties in the spray initial conditions (droplet size distribution and velocity). The SSF model shows better agreement than the DSF model because of better predictions of the droplet evaporation and spreading rates. The overestimation of temperature by the LHF model is due to the assumption of infinitely fast interphase transport.

Far downstream of the combustor inlet, all three models predict higher temperatures than the measurements. This is attributed to the neglect of radiative heat loss. Both the experimental data and the separated flow model predictions show high-temperature peaks near the combustion chamber wall at downstream locations. The peak temperatures occur in regions where droplets have traversed and evaporated. The LHF model does not predict a temperature peak near the chamber wall because this model does not consider discrete droplet motion.

Figure 3 presents the experimental data and predictions of temperatures for $S=1.98$. The temperature profiles are more uniform for $S=1.98$ than for $S=0.72$, because of the increased mixing obtained with increased swirl. The higher swirl also produces a stronger recirculating flow (i.e., more fuel vapor and hot combustion product are transported upstream) and hence higher temperatures are obtained in the upstream region for $S=1.98$. Close to the inlet at large radii, both the DSF and SSF models significantly underestimate the temperature. Very few droplet groups are predicted to arrive in this region, which is probably caused by inaccurate initial droplet velocities. The fuel vapor concentration in these regions is therefore underpredicted, which results in much lower temperatures than the experimental data. Far downstream ($X=0.52$ m) near the chamber wall, the two separated flow models significantly overestimate the temperature. This discrepancy is attributed to the assumed adiabatic wall boundary condition (as discussed earlier, wall cooling was applied in the experiment, this also applies to Fig. 2) and the errors in the calculated droplet evaporation

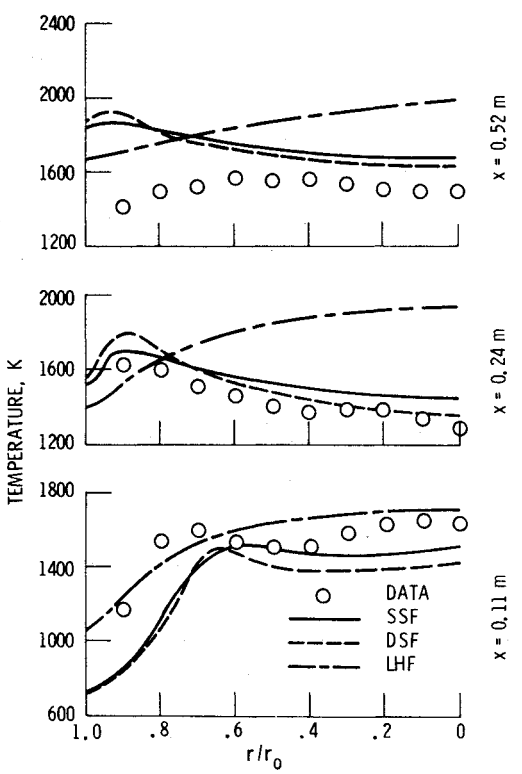


Fig. 3 Radial profiles of temperature, $S=1.98$.

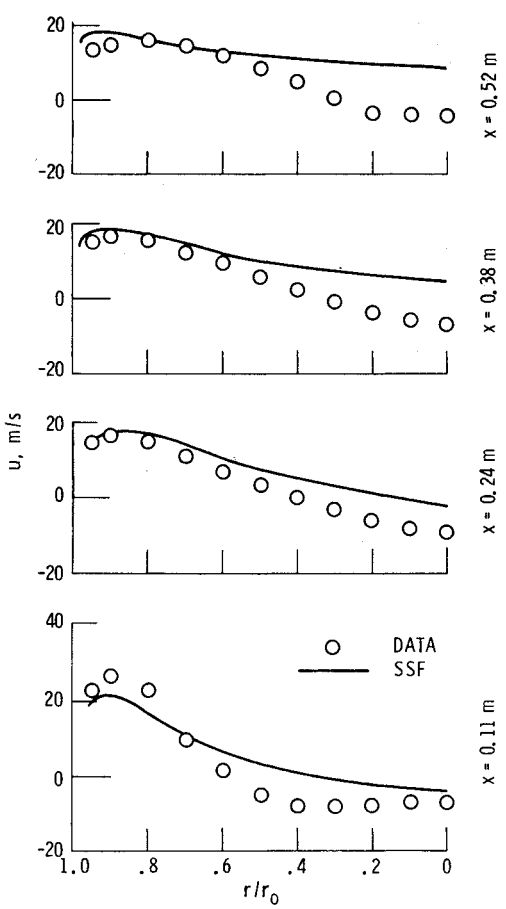


Fig. 4 Radial profiles of axial velocity, $S=1.98$.

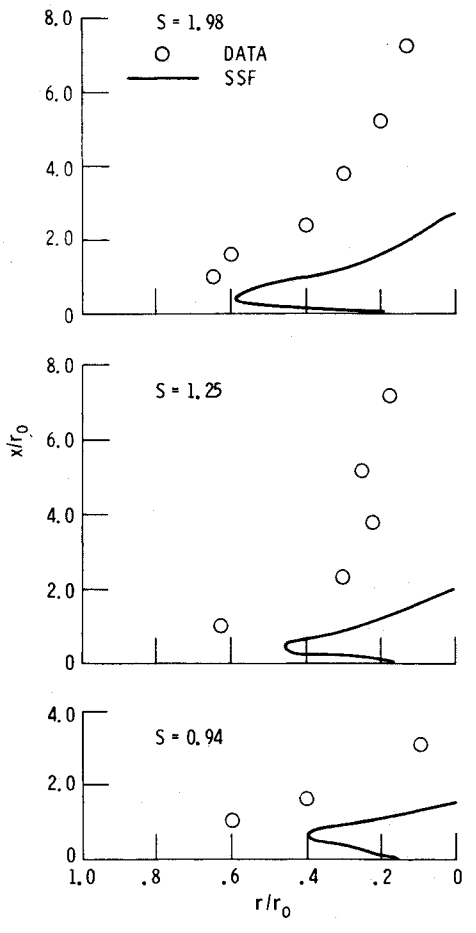


**Fig. 5 Central recirculation zone contours.**

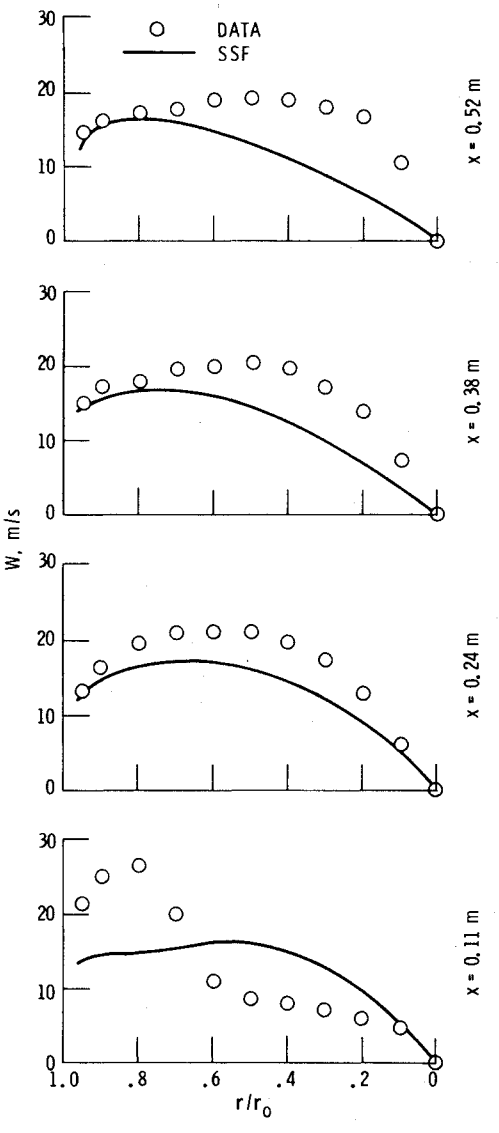


**Fig. 6 Radial profiles of tangential velocity, $S=1.98$.**

rate. While the measured temperature profiles indicate that the droplets are almost completely evaporated upstream of this region (near the wall at $X=0.52$ m), the models predict the presence of a finite amount of liquid fuel and therefore higher fuel vapor concentration and temperature in this region. For both swirl numbers in the regions downstream, the DSF model predicts higher temperature peaks, less uniform temperature distributions, and larger discrepancies compared with measurements than the SSF model (Figs. 2 and 3). This is because the DSF model neglects turbulent dispersion and underestimates droplet spreading.

Radial profiles of gas-phase axial velocity are presented in Fig. 4 for $S=1.98$. The boundaries for the central recirculation zones for $S=0.94$, 1.25, and 1.98 are shown in Fig. 5. It can be seen from Figs. 4 and 5 that both the magnitude of the reverse flow velocities and the size of the recirculation zones are underpredicted, the errors increasing with increasing swirl number. The results of this underestimation can be seen in the temperature distribution in Fig. 3. The experimental data show more uniform distributions because of greater mixing caused by larger reverse velocities. The relatively poor performance of the model in predicting the size of the central recirculation zone and the reverse velocity is partly attributed to the $k$-$\epsilon$ model used in the present analysis. It is well known that $k$-$\epsilon$ models have not been very successful in predicting highly swirling flows.[9] Beyond the central recirculation zone, the predicted axial velocities are higher than the measured values due to the higher predicted temperatures.

The predicted and measured radial profiles of gas-phase tangential velocities for $S=1.98$ are illustrated in Fig. 6. The calculated tangential velocities are smaller than the measured values at almost all locations. This discrepancy is likely caused by uncertainties in the inlet swirl velocities. It should also be noted that the swirl numbers quoted by Khalil et al.[25] for the experimental data were estimated from the swirler vane angle rather than direct measurements and may also introduce some error.

The predicted axial profiles of liquid mass flow rate are shown in Fig. 7a for $S=0.72$ and 1.98. As expected, the LHF model produces unrealistically high evaporation rates.[16] This high rate of evaporation is due to the method used to obtain the inlet boundary conditions and the assumption of infinitely fast interphase transport rates. The results of the two separated flow models appear reasonable, but the lack of experimental data prevents quantitative comparisons. The SSF model predicts higher evaporation rates than the DSF model because it considers the effects of turbulence on interphase transport, which enhances the rate of evaporation.[16,17] The influence of swirl strength on the overall evaporation rate is also clearly indicated in Fig. 7a, which shows faster evaporation for higher inlet swirl. With increased swirl, a large central recirculation zone of hot combustion products is generated and most droplets are trapped there, resulting in a high evaporation rate. In addition, the larger reverse flow recirculates more hot gas from downstream and increases the temperature at near inlet locations. This in turn contributes to a higher evaporation rate for the higher swirl case.

The predicted axial profiles of droplet SMD are illustrated in Fig. 7b for $S=0.72$. The values presented here were ob-

tained by integrating over the cross-sectional area at each axial location. As the droplets move downstream, the SMD increases and then decreases. The initial increase of SMD is caused by the reduction of the number of small droplets, due to the preferential evaporation of small droplets (i.e., small droplets evaporate faster than large droplets). When most of the small droplets have completely evaporated, the SMD begins to decrease because of the continuous evaporation of large droplets. The DSF and SSF models produce similar results, but the SSF model produces more rapid variations in the SMD than the DSF model because it predicts a higher evaporation rate.

**Measurements of El-Banhawy and Whitelaw[26]**

The experiment was conducted in a cylindrical combustion chamber equipped with a rotating cup atomizer (capable of producing a near-monodisperse spray.)[26] Liquid kerosene was used as fuel and the fuel/air mass ratio was fixed at 0.0228. Five test conditions were considered in the calculations, i.e., $(S,d_p)=(1.2, 33\ \mu m)$, $(1.2, 47\mu m)$, $(1.2, 96\ \mu m)$, $(0.7, 47\ \mu m)$, and $(0.4, 47\ \mu m)$, and are designated hereafter as runs 1-5, respectively. The swirl numbers quoted here were estimated from the swirler vane angles given in Ref. 26. In the calculations, droplets were assumed to be of uniform size with injection velocities estimated from the experimental data measured at near-atomizer locations.[26] Since the droplet sizes are relatively small, considerable change in droplet velocity can occur in the short distance between the injection location and the measurement station; therefore, some error might be introduced in the droplet initial velocity specifications. Another source of uncertainty in the calculation involves the assumption of uniform droplet size distributions. The fuel spray emerged from the atomizer in main droplets of reproducible size (which is the droplet size used in the calculation) and much smaller satellite droplets constituting around 20% of the fuel mass flow rate.[26] Since the measured droplet velocities were averaged over the droplet size and the number fraction of the smaller satellite droplets can be much greater than 20%, the specified droplet initial velocities might not be representative for the droplet sizes used in the calculation.

A schematic of the combustion chamber along with the experimentally observed spray sheet penetration[26] and the predicted recirculation zone boundaries of runs 2, 4, and 5 are shown in Fig. 8. The high swirl case (run 2) produces a large central recirculation zone and a very small corner wall recirculation region. As the swirl number decreases, the size of the central recirculation zone decreases and a relatively large wall recirculation zone is predicted. Since the shear layers enclosing the recirculation zones serve to stabilize the flames, the change in size and strength of the recirculation zones with a change in swirl number has a large impact on the overall flame structure and temperature distribution, as discussed in the following paragraph.

The measured and predicted (the DSF and SSF models) temperature contour maps for the three spray flames of runs 1-3 are shown in Figs. 9-11, respectively. Since the swirl numbers are the same for all three runs, the differences in the temperature contours are due to differences in initial droplet diameters and associated injection velocities (smaller mean droplet diameter is associated with larger injection velocity, see Ref. 26). In Figs. 9-11, two regions of high temperature are observed: 1) the shear layer around the recirculation zone and 2) the main flame region, which extends to the central recirculation zone and downstream of the fuel spray. Calculated results indicate that these high-temperature regions are characterized by the trapping of smaller droplets, high rate of evaporation, and intensive turbulent mixing and chemical reaction. Steep temperature gradients are also observed in the shear layer around the main flame region, indicating that intensive chemical reaction is taking place around here. The temperature near the rotating cup atomizer and the size of the main flame region increase with a decrease of initial mean droplet diameter for the three runs. This is due to the higher evaporation rate of the smaller

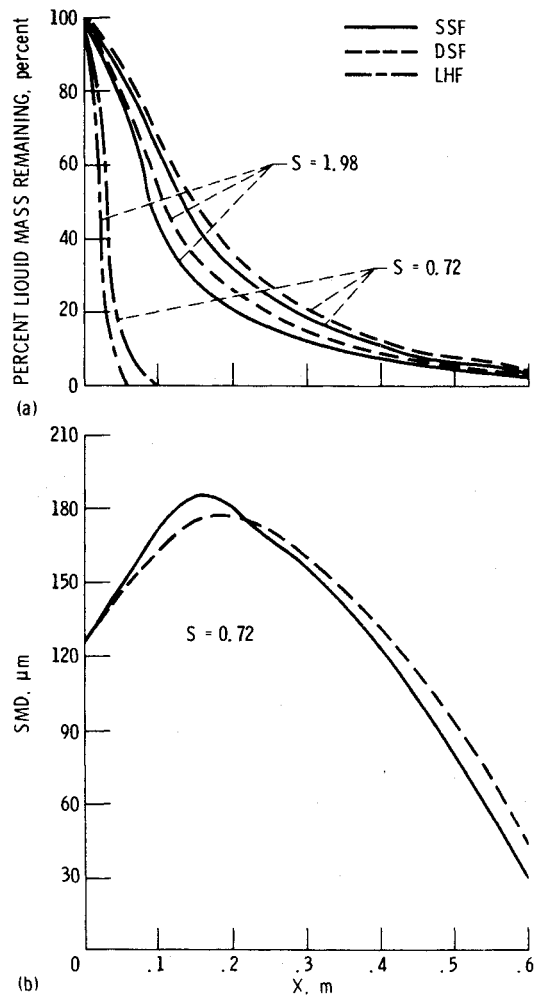


Fig. 7 Axial profiles of a) liquid mass flow rate and b) Sauter mean diameter.

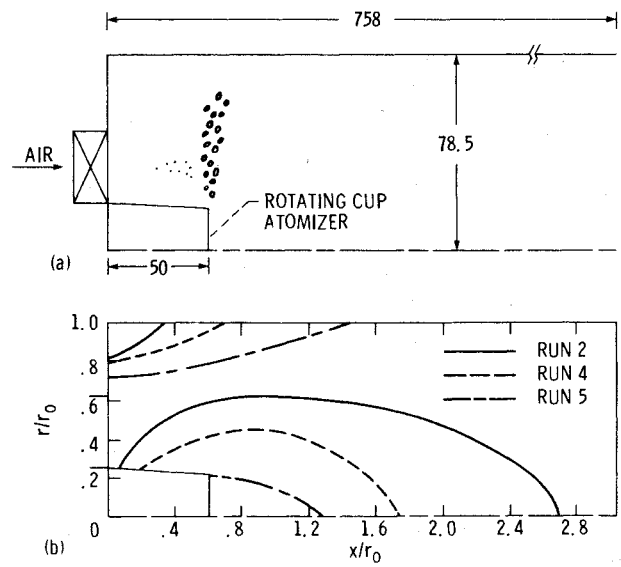


Fig. 8 a) Schematic of the combustion chamber, El-Banhawy and Whitelaw[26] (all dimensions in mm) and b) predicted recirculation zone contours.

droplets. The temperature contours in the upstream region show that the spray with a smaller mean droplet diameter penetrates deeper radially into the flow. The droplet trajectory calculations indicate that this is due to the higher injection velocities associated with smaller droplets.

Comparison of the predicted temperature contours with measurements shows that the general features of the spray flames are correctly reproduced by the models. Some quantitative discrepancies can still be observed. The size of the high-temperature main flame region is underestimated in all three runs. This is likely caused by the underprediction of the size of the central recirculation zones, which is due to the $k$-$\epsilon$ turbulence model and was discussed in the previous section. The predicted temperature gradients in the shear layer flame regions are not as steep as the measured values; this is probably caused by numerical diffusion. The neglect of radiative heat loss in the calculations yields higher temperature predictions than measurements in far downstream regions. The effect of neglecting radiation, however, is smaller in this case compared to the results shown in Figs. 2 and 3, because of the lower temperatures involved in this case due to the lower fuel/air ratio. To quantify the comparison of model predictions and measurements, the temperature profiles are integrated over the mass flow rate and cross-sectional area (the predicted mass flow rate profiles were used in integrating experimental data) at $x/r_0 = 2.8$. The difference in the averaged temperatures between the SSF model predictions and experimental data are 132, 103, and 76 K, for runs 1-3, respectively, with predictions higher than measured values in all cases.

The temperature contour maps predicted by the two separated flow models are similar, with the DSF model producing slightly more concentrated high-temperature isotherms along droplet trajectories in the upstream region. This is attributed to the neglect of droplet dispersion in the DSF model. As expected, the DSF model predicts lower temperatures than the SSF model due to the lower predicted evaporation rates, as discussed in the previous section. The largest difference occurs in run 3, where the DSF model yields an averaged temperature (integrated at $x/r_0 = 2.8$) 75 K lower than the SSF model prediction. In general, the discrepancies between the DSF and SSF predictions are smaller than those obtained in earlier studies of noncombusting flows,[13-17] since fuel droplets evaporate very fast for the present flow conditions and, therefore, the flame structure is dominated by the transport of fuel vapor rather than droplet motion and transport. The integrated temperatures at $x/r_0 = 2.8$ appear to indicate that the DSF model results agrees better with experimental data than the SSF model results. This is not true, however, since the radiative heat loss is neglected in the predictions.

The predicted (SSF model) and measured temperature contour maps for run 4 ($S = 0.7$) and run 5 ($S = 0.4$) are shown in Figs. 12 and 13. Runs 2 ($S = 1.2$, see Fig. 10), 4, and 5 all have the same initial mean droplet diameter (47 $\mu$m) and the same droplet injection velocity, but different inlet swirl numbers. Comparison of the results of the three cases can, therefore, provide useful information of the influence of swirl on spray flame structure. Some distinct features can be readily observed by comparing the temperature contour maps of the three flames. In comparison to $S = 1.2$ in run 2, the main flame region for the $S = 0.7$ case extends much further downstream and the shear layer flame shifts toward the axis of the chamber. For $S = 0.4$, the flame is characterized by lower temperatures, less steep gradients, and the shift of the flame stabilization region from the central to wall recirculation zone. These qualitative features are consistently predicted by the SSF model.

The smaller central recirculation zone caused by the reduced swirl allows the droplets to travel a greater axial distance. A close inspection of the calculated results of $S = 0.7$ shows that upon injection the droplets quickly

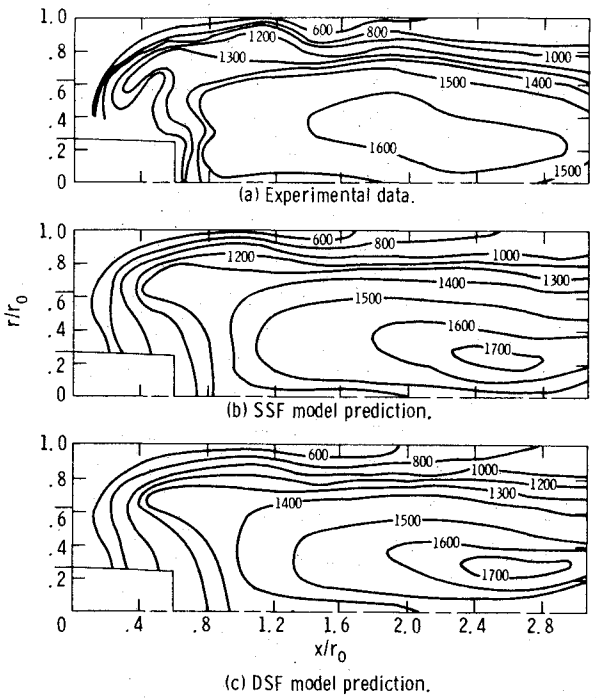


**Fig. 9 Temperature contour map, run 1 ($S = 1.2$, $dp_0 = 33$ $\mu$m, temperature in degrees K).**

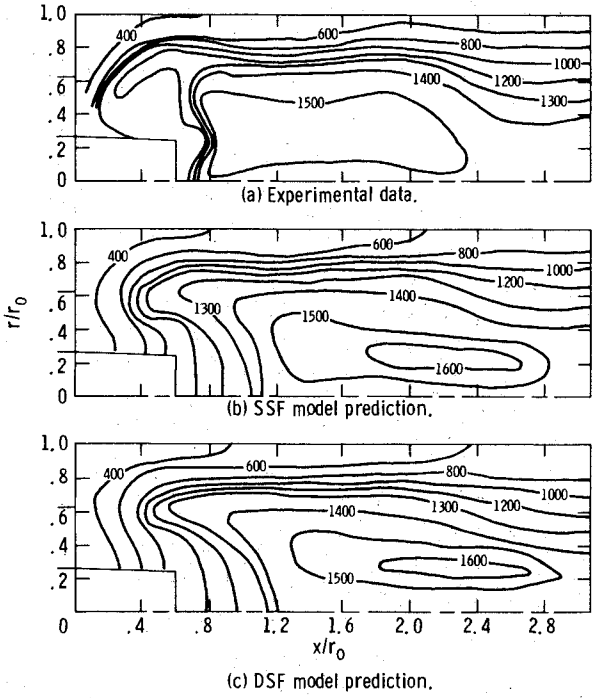


**Fig. 10 Temperature contour map, run 2 ($S = 1.2$, $dp_0 = 47$ $\mu$m, temperature in degrees K).**

penetrate the small reverse flow region around the atomizer and are then swept downstream by the high-velocity gas flow. This results in a lower evaporation rate and a shorter radial penetration distance of the droplets in upstream regions and continuous evaporation and, hence, chemical reaction in downstream regions. These effects in turn cause a longer flame length and the shifting of the upstream shear layer flame toward the axis, phenomena that are also observed in the experimental data.[26] The temperatures at small radii in the $S = 0.7$ case are lower than those for $S = 1.2$. The lower temperatures are associated with the reduction of com-

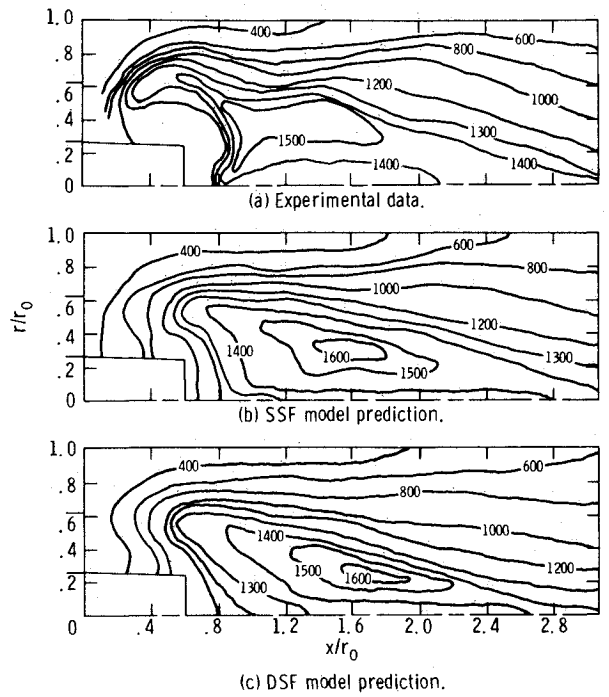


**Fig. 11 Temperature contour map, run 3 ($S=1.2$, $dp_0=96$ $\mu$m, temperature in degrees K).**

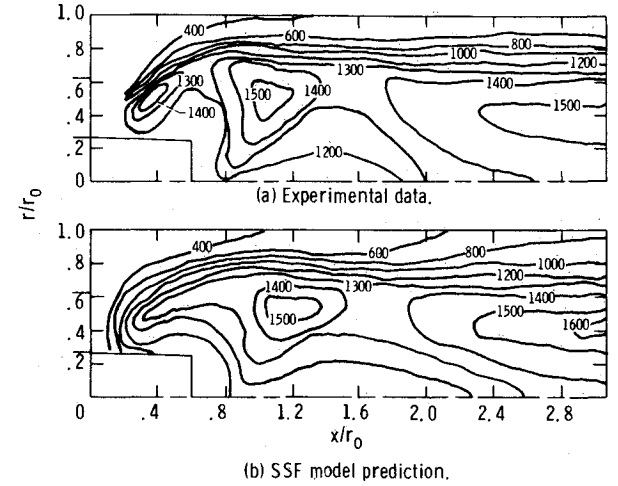


**Fig. 12 Temperature contour map, run 4 ($S=0.7$, $dp_0=47$ $\mu$m, temperature in degrees K).**

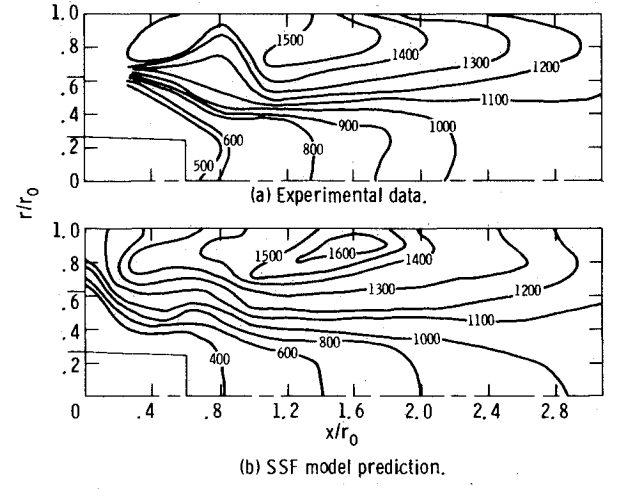


**Fig. 13 Temperature contour map, run 5 ($S=0.4$, $dp_0=47$ $\mu$m, temperature in degrees K).**

bustion intensity caused by insufficient oxygen transported to this region, as evidenced by the experimental data[26] and the calculated oxygen concentration distribution (results not shown here). The lower availability of oxygen at small radii with reduced swirl is the result of the lower turbulent mixing rate, which transports less oxygen from near wall to near axis, and the smaller central reverse flow zone, which recirculates less oxygen from downstream.

The greatly reduced turbulent mixing rates caused by low swirl in run 5 yield slow evaporation and combustion. In fact, the calculation shows that significant amount of fuel vapor and liquid droplets are still present at a large axial distance, i.e., $x/r_0>2.8$. The reduction in combustion intensity is shown by the lower temperatures and moderate temperature gradients (Fig. 13) as compared to Figs. 10 and 12. The shifting of the main flame from near the axis to the near-wall region of the $S=0.4$ case clearly demonstrates the strong influence of swirl on spray flame structure. However, it should be noted that the dramatic change in flame character shown in Fig. 13 is rather unusual and is in part a consequence of the flat spray geometry and fuel injection arrangement[26] (i.e., injecting liquid fuel tangentially from the rotating cup atomizer).

## Conclusions

Current theoretical spray models have been used to analyze fuel sprays in cylindrical combustion chambers. The LHF model yields unrealistically high evaporation rates and overestimates the development of the flow. Therefore, it has only limited utility in modeling practical sprays. In contrast, the two separated flow models yield reasonably good predictions of the general features of the spray flames. Although the SSF model appears to have certain advantages over the DSF model, the differences between the two model predictions are smaller than those observed in earlier studies of noncombusting sprays[13-17] and are comparable to uncertainties in the measurements, similar to the findings by Gosman and Ioannides.[8]

The effects of the inlet swirl strength and droplet size on spray flame structure are significant for flows considered in the present study. Strong swirl is found to produce a high rate of evaporation and intensive turbulent mixing and combustion. An increase in initial droplet diameter causes a reduction of combustion intensity and longer flame length.

## Acknowledgment

This research was sponsored by the National Aeronautics and Space Administration, Contract NAS 3-24105, under the technical management of Daniel L. Bulzan of the Lewis Research Center.

## References

[1]Crowe, C.T., "Review-Numerical Models for Dilute Gas-Particle Flows," *Journal of Fluids Engineering,* Vol. 104, No. 3, Sept. 1982, pp. 297-303.

[2]Law, C.K., "Recent Advances in Droplet Vaporization and Combustion," *Progress in Energy and Combustion Science,* Vol. 8, 1982, pp. 171-201.

[3]Faeth, G.M., "Evaporization and Combustion of Sprays," *Progress in Energy and Combustion Science,* Vol. 9, 1983, pp. 1-76.

[4]Sirignano, W.A., "Fuel Vaporization and Spray Combustion Theory," *Progress in Energy and Combustion Science,* Vol. 9, 1983, pp. 291-322.

[5]Shearer, A.J., Tamura, H., and Faeth, G.M., "Evaluation of a Locally Homogeneous Flow Model of Spray Evaporation," *Journal of Energy,* Vol. 3, Sept.-Oct. 1979, pp. 271-278.

[6]Khalil, E.E. and Whitelaw, J.H., "Aerodynamic and Thermodynamic Characteristics of Kerosene-Spray Flame," *Sixteenth Symposium (International) on Combustion,* The Combustion Institute, Pittsburgh, PA, 1977, pp. 569-576.

[7]Gosman, A.D. and Johns, R.J.R., "Computer Analysis of Fuel-Air Mixing in Direct-Injection Engines," *Diesel Combustion and Emissions,* SEA P-86, SAE, Warrendale, PA, 1980, pp. 75-90.

[8]Gosman, A.D. and Ioannides, E., "Aspects of Computer Simulation of Liquid-Fueled Combustors," *Journal of Energy,* Vol. 7, Nov-Dec. 1983, pp. 482-490.

[9]El-Banhawy, Y. and Whitelaw, J.H., "Calculation of the Flow Properties of a Confined Kerosene-Spray Flame," *AIAA Journal,* Vol. 18, Dec. 1980, pp. 1503-1510.

[10]Williams, F.A., *Combustion Theory,* Addison-Wesley, Reading, MA, 1965.

[11]Gosman, A.D., Ioannides, E., Lever, D.A., and Cliffe, K.A., "A Comparison of Continuum and Discrete Droplet Finite-Difference Models Used in the Calculation of Spray Combustion in Swirling Turbulent Flows," AERE TP-865, July 1980.

[12]Dukowicz, J.K., "A Particle-Fluid Numerical Model for Liquid Sprays," *Journal of Computational Physics,* Vol. 35, No. 2, April 1980, pp. 229-253.

[13]Shuen, J.-S., Solomon, A.S.P., Zhang, Q.-F., and Faeth, G.M., "Structure of Particle-Laden Jets: Measurements and Predictions," *AIAA Journal,* Vol. 23, March 1985, pp. 396-404.

[14]Solomon, A.S.P., Shuen, J.-S., Zhang, Q.-F., and Faeth, G.M., "Structure of Nonevaporating Sprays, Part I: Initial Conditions and Mean Properties," *AIAA Journal,* Vol. 23, Oct. 1985, pp. 1548-1555.

[15]Solomon, A.S.P., Shuen, J.-S., Zhang, Q.F., and Faeth, G.M., "Structure of Nonevaporating Sprays, Part II: Drop and Turbulence Properties," *AIAA Journal,* Vol. 23, Nov. 1985, pp. 1724-1730.

[16]Solomon, A.S.P., Shuen, J.-S., Zhang, Q.-F., and Faeth, G.M., "Measurements and Predictions of the Structure of Evaporating Sprays," *Journal of Heat Transfer,* Vol. 107, No. 3, Aug. 1985, pp. 679-686.

[17]Shuen, J.-S., Solomon, A.S.P., and Faeth, G.M., "Drop-Turbulence Interactions in a Diffusion Flame," *AIAA Journal,* Vol. 24, Jan. 1986, pp. 101-108.

[18]Onuma, Y., Ogasawara, M., and Inoue, T., "Further Experiments on the Structure of a Spray Combustion Flame," *Sixteenth Symposium (International) on Combustion,* The Combustion Institute, Pittsburgh, PA, 1977, pp. 561-567.

[19]Gordon, S., and McBride, B.J., "Computer Program for Calculation of Complex Chemical Equilibrium Compositions, Rocket Performance, Incident and Reflected Shock, and Chapman-Jouget Detonations," NASA SP-273, 1976.

[20]Jeng, S.M. and Faeth, G.M., "Species Concentrations and Turbulence Properties in Buoyant Methane Diffusion Flames," *Journal of Heat Transfer,* Vol. 106, No. 4, Nov. 1984, pp. 721-727.

[21]Mao, C.-P., Szekely, G.A. Jr., and Faeth, G.M., "Evaluation of a Locally Homogeneous Flow Model of Spray Combustion," NASA CR-3202, April 1980.

[22]Bilger, R.W., "Turbulent Jet Diffusion Flames," *Progress in Energy and Combustion Science,* Vol. 1, 1976, pp. 87-109.

[23]Syed, S.A., Chiappetta, L.J., and Gosman, A.D., "Error Reduction Program—Final Report," NASA CR-174776, Jan. 1985.

[24]Issa, R.I., "Numerical Methods for Two- and Three-Dimensional Recirculating Flows," *Computational Methods for Turbulent, Transonic, and Viscous Flows,* edited by J.A. Essers, Hemisphere Publishing, New York, 1983, pp. 183-212.

[25]Khalil, K.H., El-Mahallawy, F.M., and Moneib, H.A., "Effect of Combustion Air Swirl on the Flow Pattern in a Cylindrical Oil Fired Furnace," *Sixteenth Symposium (International) on Combustion,* The Combustion Institute, Pittsburgh, PA, 1977, pp. 135-143.

[26]El-Banhawy, Y. and Whitelaw, J.H., "Experimental Study of the Interaction Between a Fuel Spray and Surrounding Combustion Air," *Combustion and Flame,* Vol. 42, No. 3, Sept. 1981, pp. 253-275.